

# Mathematical analysis of the quasilinear effects in a hyperbolic model blood flow through compliant axi-symmetric vessels

Sunčica Čanić<sup>1,\*</sup> and Eun Heui Kim<sup>2</sup>

<sup>1</sup>*Department of Mathematics, University of Houston, Houston, TX 77204-3476, U.S.A.*

<sup>2</sup>*Department of Mathematics, California State University, Long Beach, CA 90840-1001, U.S.A.*

Communicated by H. A. Levine

## SUMMARY

In this paper, we present a mathematical analysis of the quasilinear effects arising in a hyperbolic system of partial differential equations modelling blood flow through large compliant vessels. The equations are derived using asymptotic reduction of the incompressible Navier–Stokes equations in narrow, long channels.

To guarantee strict hyperbolicity we first derive the estimates on the initial and boundary data which imply strict hyperbolicity in the region of smooth flow. We then prove a general theorem which provides conditions under which an initial–boundary value problem for a quasilinear hyperbolic system admits a smooth solution. Using this result we show that pulsatile flow boundary data always give rise to shock formation (high gradients in the velocity and inner vessel radius). We estimate the time and the location of the first shock formation and show that in a healthy individual, shocks form well outside the physiologically interesting region (2.8 m downstream from the inlet boundary). In the end we present a study of the influence of vessel tapering on shock formation. We obtain a surprising result: vessel tapering postpones shock formation. We provide an explanation for why this is the case. Copyright © 2003 John Wiley & Sons, Ltd.

KEY WORDS: hemodynamics; hyperbolic conservation laws; shock formation

## 1. INTRODUCTION

A simple one-dimensional model of blood flow through axi-symmetric compliant vessels (14) has been used by many authors to study various issues related to the vascular system [1–5,25]. The simplicity of the model makes it useful in fast real-time computations when quick answers are needed in the cases when the geometry of the patient's vessel can be approximated

---

\*Correspondence to: Sunčica Čanić, Department of Mathematics, University of Houston, Houston, TX 77204-3476, U.S.A.

Contract/grant sponsor: National Science Foundation; contract/grant number: DMS-9970310

Contract/grant sponsor: Texas Higher Education Board (ARP Mathematics); contract/grant number: 003652-0112-2001

Contract/grant sponsor: National Science Foundation; contract/grant number: DMS-0103823

by a straight, narrow, compliant wall channel. The model has been used, for example, in the computation of blood flow through the aorta and coupled to the 3D and lumped models to simulate the entire human vascular system [3]; using a 'structured tree' to simulate the 'arterial tree', the one-dimensional model is the basis for the numerical simulations presented in Reference [4]; assuming variable Young's modulus this model has been used in References [6,7] to study properties of blood flow and the optimal design of stents (prostheses) in the endovascular treatment of abdominal aneurysm; in Reference [8] variable Young's modulus and the one-dimensional equations have been implemented to study endovascular treatment of stenosis.

In spite of the appearance in a wide literature, we have found that there are several issues related to the stability and singularity formation that have either not been known or that have not been completely understood. In this paper, we present a comprehensive rigorous mathematical analysis of the underlying quasilinear partial differential equations with the initial and boundary data that correspond to pulsatile blood flow in large vessels. The results of this paper can be summarized as follows.

1. We present a rigorous derivation of the equations which are obtained using asymptotic analysis of the incompressible Navier–Stokes equations in narrow, long channels; see Reference [8] for basic reference.
2. We derive the conditions on the initial and boundary data that provide strict hyperbolicity of the equations in the region of smooth flow. (Although strict hyperbolicity of the equations is assumed everywhere in the literature, it is not true that the problem will be strictly hyperbolic for any initial and boundary data.)
3. We prove a general theorem, stated in the form which can easily be applied to the underlying equations, which provides the conditions under which an initial–boundary value problem for a hyperbolic system of partial differential equations has a smooth solution.
4. We use this theorem to prove that pulsatile boundary data will always lead to shock formation in an idealized blood vessel that is very long and straight. We estimate the time and location of first shock formation in the blood flow problem and show that in a healthy individual, shocks develop well outside the physiologically relevant domain.
5. We use numerical simulations together with the derived estimates to study shock formation in tapering vessels. We obtain a surprising result which shows that tapering causes delay in the first shock formation. We provide an explanation for why this is the case.

## 2. THE DERIVATION OF THE MODEL EQUATIONS

Although various versions of the equations we study in this paper have been used by many authors to model blood flow through compliant vessels, we have found that the derivation of the equations studied here has not always been described in a satisfactory manner. As a consequence, the source terms describing the viscous effects in axisymmetric, narrow and long vessels, have different forms in different literature sources. For the sake of completeness and correctness, we include the derivation of the equations here.

There are a couple of different approaches one can take to obtain the underlying equations using asymptotic reduction from the full set of incompressible Navier–Stokes equation in narrow, long channels. One is based on *a priori* estimates, and the other on the

non-dimensionalization of the underlying equations. In this paper we take the latter approach. We will perform asymptotic reduction of the equations in non-dimensional variables by ignoring the terms of order  $\varepsilon^2$  and smaller, where  $\varepsilon$  is the ratio of the width vs the length of the channel. Essentially this is what was done in Reference [8].

We start with the incompressible axisymmetric Navier–Stokes equations in cylindrical coordinates  $(x, r, \theta)$ . The  $x$  co-ordinate is aligned with the axis of symmetry of the channel. Denote the velocity components by  $V = (V_x, V_r, V_\theta)$ . We first assume that the angular velocity is zero to obtain the following equations of motion:

$$\begin{aligned} \frac{\partial V_x}{\partial t} + V_r \frac{\partial V_x}{\partial r} + V_x \frac{\partial V_x}{\partial x} + \frac{1}{\rho} \frac{\partial p}{\partial x} &= \nu \left[ \frac{\partial^2 V_x}{\partial r^2} + \frac{1}{r} \frac{\partial V_x}{\partial r} + \frac{\partial^2 V_x}{\partial x^2} \right] \\ \frac{\partial V_r}{\partial t} + V_r \frac{\partial V_r}{\partial r} + V_x \frac{\partial V_r}{\partial x} + \frac{1}{\rho} \frac{\partial p}{\partial r} &= \nu \left[ \frac{\partial^2 V_r}{\partial r^2} + \frac{1}{r} \frac{\partial V_r}{\partial r} - \frac{V_r}{r^2} + \frac{\partial^2 V_r}{\partial x^2} \right] \end{aligned}$$

and the incompressibility condition

$$\frac{\partial V_x}{\partial x} + \frac{1}{r} \frac{\partial(r V_r)}{\partial r} = 0 \quad (1)$$

### 2.1. The reduced non-dimensional equations

Introduce the following characteristic quantities:

- $U_0$  and  $V_0$  are the characteristic radial and axial velocities,
- $\lambda$  is the characteristic length, and  $R_0$  is the characteristic inner vessel radius, and the corresponding non-dimensional variables:
- $r = R_0 \tilde{r}$ ,  $x = \lambda \tilde{x}$ ,  $t = \frac{\lambda}{V_0} \tilde{t}$ ,  $V_x = V_0 \tilde{V}_x$ ,  $V_r = U_0 \tilde{V}_r$ ,  $p = \rho V_0^2 \tilde{p}$

Notice that

$$\frac{R_0}{\lambda} = \frac{U_0}{V_0} \quad (2)$$

which is the small parameter  $\varepsilon$ . (In the flow regime corresponding to the abdominal aorta between the renal and iliac arteries, the ratio between the radius and the length is of order  $\mathcal{O}(10^{-2})$ .)

The incompressibility condition in non-dimensional variables reads

$$\frac{1}{R_0} \frac{\partial}{\partial \tilde{r}} (R_0 \tilde{r} U_0 \tilde{V}_r) + \frac{1}{\lambda} \frac{\partial}{\partial \tilde{x}} (R_0 \tilde{r} V_0 \tilde{V}_x) = 0$$

or

$$\frac{\partial}{\partial \tilde{r}} (\tilde{r} \tilde{V}_r) + \frac{V_0 R_0}{U_0 \lambda} \frac{\partial}{\partial \tilde{x}} (\tilde{r} \tilde{V}_x) = 0$$

Noting that  $V_0 R_0 / U_0 \lambda = 1$  we obtain

$$\frac{\partial}{\partial \tilde{r}} (\tilde{r} \tilde{V}_r) + \frac{\partial}{\partial \tilde{x}} (\tilde{r} \tilde{V}_x) = 0 \quad (3)$$

The first momentum equation in non-dimensional variables becomes

$$\begin{aligned} & \frac{V_0}{\lambda} \frac{\partial}{\partial \tilde{t}} (V_0 \tilde{V}_x) + U_0 \tilde{V}_r \frac{1}{R_0} \frac{\partial}{\partial \tilde{r}} (V_0 \tilde{V}_x) + V_0 \tilde{V}_x \frac{1}{\lambda} \frac{\partial}{\partial \tilde{x}} (V_0 \tilde{V}_x) + \frac{1}{\rho} \frac{V_0^2 \rho}{\lambda} \frac{\partial \tilde{p}}{\partial \tilde{x}} \\ &= v \left[ \frac{1}{R_0^2} V_0 \frac{\partial^2 \tilde{V}_x}{\partial \tilde{r}^2} + \frac{V_0}{R_0} \frac{1}{\tilde{r}} \frac{1}{R_0} \frac{\partial \tilde{V}_x}{\partial \tilde{r}} + \frac{V_0}{\lambda^2} \frac{\partial^2 \tilde{V}_x}{\partial \tilde{x}^2} \right] \end{aligned}$$

After dividing this equation by  $V_0^2$  and multiplying by  $\lambda$  we obtain

$$\frac{\partial \tilde{V}_x}{\partial \tilde{t}} + \frac{U_0}{R_0} \frac{\lambda}{V_0} \tilde{V}_r \frac{\partial \tilde{V}_x}{\partial \tilde{r}} + \tilde{V}_x \frac{\partial \tilde{V}_x}{\partial \tilde{x}} + \frac{\partial \tilde{p}}{\partial \tilde{x}} = \frac{v\lambda}{V_0 R_0^2} \left[ \frac{\partial^2 \tilde{V}_x}{\partial \tilde{r}^2} + \frac{1}{\tilde{r}} \frac{\partial \tilde{V}_x}{\partial \tilde{r}} + \frac{R_0^2}{\lambda^2} \frac{\partial^2 \tilde{V}_x}{\partial \tilde{x}^2} \right]$$

Take into account that  $(U_0/R_0)\lambda/V_0 = 1$ . Then notice that the last term is of order  $\varepsilon^2$  and neglect it. For the problem describing blood flow in the abdominal aorta between the renal and iliac arteries, the characteristic variables typically take the following values:

$$v = 3.2 \times 10^{-6} \text{ m}^2/\text{s}, \quad R_0 = 0.0082 \text{ m}, \quad \lambda = 0.1 \text{ m} \quad \text{and} \quad V_0 \approx 0.1 \text{ m/s}$$

so that the coefficient in front of the right-hand side is of order  $\mathcal{O}(10^{-1})$  and we keep it since it is larger than  $\varepsilon$  (and, of course,  $\varepsilon^2$ ).

After neglecting the term of order  $\varepsilon^2$  we multiply the above equation by  $\tilde{r}$  to obtain

$$\tilde{r} \frac{\partial \tilde{V}_x}{\partial \tilde{t}} + \tilde{r} \tilde{V}_r \frac{\partial \tilde{V}_x}{\partial \tilde{r}} + \tilde{r} \tilde{V}_x \frac{\partial \tilde{V}_x}{\partial \tilde{x}} + \tilde{r} \frac{\partial \tilde{p}}{\partial \tilde{x}} = \frac{v\lambda}{V_0 R_0^2} \left[ \frac{\partial}{\partial \tilde{r}} \left( \tilde{r} \frac{\partial \tilde{V}_x}{\partial \tilde{r}} \right) \right]$$

We rewrite the left-hand side in conservation form by calculating

$$\begin{aligned} \frac{\partial}{\partial \tilde{r}} (\tilde{r} \tilde{V}_r \tilde{V}_x) &= \tilde{V}_x \frac{\partial}{\partial \tilde{r}} (\tilde{r} \tilde{V}_r) + \tilde{r} \tilde{V}_r \frac{\partial \tilde{V}_x}{\partial \tilde{r}} \\ \frac{\partial}{\partial \tilde{x}} (\tilde{r} \tilde{V}_x^2) &= \tilde{V}_x \frac{\partial}{\partial \tilde{x}} (\tilde{r} \tilde{V}_x) + \tilde{r} \tilde{V}_x \frac{\partial \tilde{V}_x}{\partial \tilde{x}} \end{aligned} \quad (4)$$

and by using the incompressibility condition to observe that the first terms on the right-hand side are the same but with opposite sign. Using (4) the terms on the left-hand side of the first momentum equation can be written in the conserved form to obtain the reduced first momentum equation in non-dimensional variables

$$\frac{\partial}{\partial \tilde{t}} (\tilde{r} \tilde{V}_x) + \frac{\partial}{\partial \tilde{r}} (\tilde{r} \tilde{V}_r \tilde{V}_x) + \frac{\partial}{\partial \tilde{x}} (\tilde{r} \tilde{V}_x^2) + \frac{\partial}{\partial \tilde{x}} (\tilde{r} \tilde{p}) = \frac{v\lambda}{V_0 R_0^2} \left[ \frac{\partial}{\partial \tilde{r}} \left( \tilde{r} \frac{\partial \tilde{V}_x}{\partial \tilde{r}} \right) \right] \quad (5)$$

The second momentum equation in non-dimensional variables reads

$$\begin{aligned} & \frac{V_0}{\lambda} \frac{\partial}{\partial \tilde{t}} (U_0 \tilde{V}_r) + U_0 \tilde{V}_r \frac{1}{R_0} \frac{\partial}{\partial \tilde{r}} (U_0 \tilde{V}_r) + V_0 \tilde{V}_x \frac{1}{\lambda} \frac{\partial}{\partial \tilde{x}} (U_0 \tilde{V}_r) + \frac{1}{\rho} \frac{1}{R_0} \frac{\partial}{\partial \tilde{r}} (\rho V_0^2 \tilde{p}) \\ &= v \left[ \frac{1}{R_0^2} \frac{\partial^2}{\partial \tilde{r}^2} (U_0 \tilde{V}_r) + \frac{1}{R_0^2} \frac{1}{\tilde{r}} \frac{\partial}{\partial \tilde{r}} (U_0 \tilde{V}_r) - \frac{U_0 \tilde{V}_r}{R_0^2 \tilde{r}^2} + \frac{1}{\lambda^2} \frac{\partial^2}{\partial \tilde{x}^2} (U_0 \tilde{V}_r) \right] \end{aligned}$$

Divide this equation by  $V_0^2$  and multiply by  $R_0$  to obtain

$$\begin{aligned} & \frac{R_0}{\lambda} \frac{U_0}{V_0} \frac{\partial}{\partial \tilde{t}} (\tilde{V}_r) + \frac{U_0^2}{V_0^2} \tilde{V}_r \frac{\partial}{\partial \tilde{t}} (\tilde{V}_r) + \frac{R_0}{\lambda} \frac{U_0}{V_0} \frac{\partial}{\partial \tilde{x}} (\tilde{V}_r) + \frac{\partial \tilde{p}}{\partial \tilde{r}} \\ &= v \left[ \frac{1}{R_0} \frac{U_0}{V_0^2} \frac{\partial^2 \tilde{V}_r}{\partial \tilde{r}^2} + \frac{1}{R_0} \frac{U_0}{V_0^2} \frac{1}{\tilde{r}^2} \frac{\partial}{\partial \tilde{t}} (\tilde{V}_r) - \frac{U_0}{V_0^2} \frac{\tilde{V}_r}{R_0 \tilde{r}^2} + \frac{R_0}{\lambda^2} \frac{U_0}{V_0^2} \frac{\partial^2 \tilde{V}_r}{\partial \tilde{x}^2} \right] \end{aligned}$$

Since  $R_0/\lambda = U_0/V_0 = \varepsilon$  all the terms in the above expression are of order  $\varepsilon^2$  except for the pressure term, and so, after ignoring the terms of order  $\varepsilon^2$  the equation becomes

$$\frac{\partial \tilde{p}}{\partial \tilde{r}} = 0 \quad (6)$$

Therefore, the reduced second momentum equation implies that the pressure is constant across the vessel cross-section.

## 2.2. The averaged equations

We next express these equations in terms of the averaged quantities across the cross-sectional area. Let  $\tilde{R}$  denote the inner vessel radius. We introduce

$$\begin{aligned} \tilde{U} &= \frac{1}{\tilde{R}^2} \int_0^{\tilde{R}} 2\tilde{V}_x \tilde{r} d\tilde{r} \\ \alpha &= \frac{1}{\tilde{R}^2 \tilde{U}^2} \int_0^{\tilde{R}} 2\tilde{V}_x^2 \tilde{r} d\tilde{r} \end{aligned}$$

$\tilde{U}$  is the averaged axial velocity and  $\alpha$  is the ‘correction term’ or the ‘Coriolis coefficient’ [3] which takes into account the fact that the resulting momentum equation will express conservation of the averaged momentum and not the actual momentum. When the velocity profile  $\tilde{V}_x$  is independent of  $x$  the term  $\alpha$  is constant.

We will integrate the governing equations from  $\tilde{r}=0$  to  $\tilde{R}$  and express them in terms of the averaged quantities. At this point, we need to specify the boundary condition at the wall where  $\tilde{r}=\tilde{R}$ . In this paper we will be assuming the streamline condition

$$[\tilde{V}_r]_{\tilde{r}=\tilde{R}} = \frac{\partial \tilde{R}}{\partial \tilde{x}} [\tilde{V}_x]_{\tilde{r}=\tilde{R}} + \frac{\partial \tilde{R}}{\partial \tilde{t}} \quad (7)$$

*The incompressibility condition:* We integrate Equation (3) to obtain

$$[\tilde{r}\tilde{V}_r]_{\tilde{r}=\tilde{R}} + \frac{\partial}{\partial \tilde{x}} \int_0^{\tilde{R}} (\tilde{r}\tilde{V}_x) d\tilde{r} - \frac{\partial \tilde{R}}{\partial \tilde{x}} [\tilde{r}\tilde{V}_x]_{\tilde{r}=\tilde{R}} = 0$$

By taking into account the definition of  $\tilde{U}$  we get

$$\tilde{R}[\tilde{V}_r]_{\tilde{r}=\tilde{R}} + \frac{\partial}{\partial \tilde{x}} \left( \tilde{U} \frac{\tilde{R}^2}{2} \right) - \tilde{R} \frac{\partial \tilde{R}}{\partial \tilde{x}} [\tilde{V}_x]_{\tilde{r}=\tilde{R}} = 0 \quad (8)$$

The streamline condition now implies

$$\tilde{R} \frac{\partial \tilde{R}}{\partial \tilde{t}} + \frac{\partial}{\partial \tilde{x}} \left( \tilde{U} \frac{\tilde{R}^2}{2} \right) = 0$$

or, written in conservation form

$$\frac{\partial}{\partial \tilde{t}} \tilde{R}^2 + \frac{\partial}{\partial \tilde{x}} (\tilde{R}^2 \tilde{U}) = 0 \quad (9)$$

*The first momentum equation:* Integrate the reduced first momentum equation to obtain

$$\begin{aligned} & \frac{\partial}{\partial \tilde{t}} \int_0^{\tilde{R}} \tilde{r} \tilde{V}_x \, d\tilde{r} - \tilde{R} [\tilde{V}_x]_{\tilde{r}=\tilde{R}} \frac{\partial \tilde{R}}{\partial \tilde{t}} + \tilde{R} [\tilde{V}_r \tilde{V}_x]_{\tilde{r}=\tilde{R}} \\ & + \frac{\partial}{\partial \tilde{x}} \int_0^{\tilde{R}} \tilde{r} \tilde{V}_x^2 \, d\tilde{r} - \tilde{R} \tilde{V}_x^2 \frac{\partial \tilde{R}}{\partial \tilde{x}} + \int_0^{\tilde{R}} \tilde{r} \frac{\partial \tilde{p}}{\partial \tilde{x}} = \frac{\nu \lambda}{V_0 R_0^2} \tilde{R} \left[ \frac{\partial \tilde{V}_x}{\partial \tilde{r}} \right]_{\tilde{r}=\tilde{R}} \end{aligned}$$

We factor out  $\tilde{R} [\tilde{V}_x]_{\tilde{r}=\tilde{R}}$  from the three terms that contain this factor and notice that the resulting terms comprise the left-hand side of the streamline condition (7). Also notice that  $\tilde{p}$  is independent of  $\tilde{r}$  and the integral involving the pressure can be calculated. Furthermore, if we recall the definitions of the averaged quantities we finally obtain

$$\frac{\partial}{\partial \tilde{t}} \left( \frac{\tilde{R}^2}{2} \tilde{U} \right) + \frac{\partial}{\partial \tilde{x}} \left( \frac{\alpha \tilde{R}^2 \tilde{U}^2}{2} \right) + \frac{\tilde{R}^2}{2} \frac{\partial \tilde{p}}{\partial \tilde{x}} = \frac{\nu \lambda}{V_0 R_0^2} \tilde{R} \left[ \frac{\partial \tilde{V}_x}{\partial \tilde{r}} \right]_{\tilde{r}=\tilde{R}}$$

We summarize the non-dimensionalized, averaged, reduced equations

$$\begin{aligned} & \frac{\partial}{\partial \tilde{t}} \tilde{R}^2 + \frac{\partial}{\partial \tilde{x}} (\tilde{R}^2 \tilde{U}) = 0 \\ & \frac{\partial}{\partial \tilde{t}} (\tilde{R}^2 \tilde{U}) + \frac{\partial}{\partial \tilde{x}} (\alpha \tilde{R}^2 \tilde{U}^2) + \tilde{R}^2 \frac{\partial \tilde{p}}{\partial \tilde{x}} = 2 \frac{\nu \lambda}{V_0 R_0^2} \tilde{R} \left[ \frac{\partial \tilde{V}_x}{\partial \tilde{r}} \right]_{\tilde{r}=\tilde{R}} \end{aligned}$$

Keep in mind that the viscous term on the right-hand side of the momentum equation is one order of magnitude smaller than all the other terms.

### 2.3. The reduced, averaged equations in dimensional form

We define the averaged cross-sectional velocity  $U$  and the correction coefficient  $\alpha$  and find their relationship with the non-dimensional quantities.

The averaged axial velocity  $\tilde{U}$  expressed in terms of the dimensional quantities equals

$$\tilde{U} = \frac{R_0^2}{R^2} \int_0^R 2 \frac{r}{R_0} \frac{1}{V_0} V_x \frac{1}{R_0} \, dr = \frac{2}{V_0 R^2} \int_0^R r V_x \, dr$$

where  $R$  is the inner vessel radius in dimensional variables. We define the dimensional axial velocity

$$U = \frac{1}{R^2} \int_0^R 2rV_x \, dr$$

and obtain

$$U = V_0 \tilde{U}$$

which is consistent with the axial velocity component transformation.

A similar calculation gives

$$\alpha = \frac{1}{R^2 U^2} \int_0^R 2V_x^2 r \, dr \quad (10)$$

Using these definitions we transform the reduced equations back to their dimensional form to obtain

$$\begin{aligned} \frac{\partial R^2}{\partial t} + \frac{\partial}{\partial x}(R^2 U) &= 0 \\ \frac{\partial}{\partial t}(R^2 U) + \frac{\partial}{\partial x}(\alpha R^2 U^2) + \frac{R^2}{\rho} \frac{\partial p}{\partial x} &= 2\nu R \left[ \frac{\partial V_x}{\partial r} \right]_{r=R} \end{aligned} \quad (11)$$

#### 2.4. The viscous term

To obtain the equations written in terms of the averaged quantities we need to specify the axial velocity profile  $V_x$ . If we assume that the profile is independent of the position  $x$ , then the viscous term will be homogeneous, and this will also lead to  $\alpha$  being a constant.

A typical approximation for the velocity profile is

$$V_x = \frac{\gamma + 2}{\gamma} U \left[ 1 - \left( \frac{r}{R} \right)^\gamma \right] \quad (12)$$

(Hagen–Poiseuille flow, see e.g. Reference [9]).

Notice that  $\gamma=2$  corresponds to the Newtonian fluid.  $\gamma=9$  is closer to the ‘plug flow’ profile; it describes the flow of a non-Newtonian fluid reflecting the fact that blood is a suspension of cellular elements (mostly red blood cells) in plasma. It has been reported in References [10,11] that  $\gamma=9$  is a good compromise fit to the experimental data.  $\gamma=9$  leads to  $\alpha=1.1$ . Namely, (10) and (12) imply the following relationship between the shape of the velocity profile determined by  $\gamma$  and the correction coefficient  $\alpha$ :

$$\gamma = \frac{2 - \alpha}{\alpha - 1}$$

We can now differentiate the term on the right-hand side of the momentum equation in (11) to obtain that the right-hand side equals

$$f_v = 2\nu R \left( -\frac{(\gamma + 2)U}{R} \right) = -2(\gamma + 2)\nu U \quad (13)$$

We remark that in the blood-flow applications the velocity profile  $V_x$  depends on both  $x$  and  $t$  and this is one place where the current model can be generalized. Analysis which will study the influence of the spatial and temporal variations in the velocity profile from (12) on the leading order fluid-structure dynamics has not been performed and is an interesting topic of further research.

### 2.5. The equations in dimensional form in terms of the conserved quantities

Introduce the (scaled) cross-sectional area  $A = R^2$  and the momentum based on the averaged velocity  $m = AU$  and write the equations which describe conservation of mass and momentum

$$\begin{aligned} \frac{\partial A}{\partial t} + \frac{\partial m}{\partial x} &= 0 \\ \frac{\partial m}{\partial t} + \frac{\partial}{\partial x} \left( \frac{\alpha m^2}{A} \right) + \frac{A}{\rho} \frac{\partial p}{\partial x} &= -2 \frac{\alpha}{\alpha - 1} v \frac{m}{A} \end{aligned} \quad (14)$$

To close the system, the pressure term needs to be specified. This is where the distensibility of the blood vessels comes into play. In this paper we use the ‘independent ring model’ [12–15]. This model can be obtained from the Navier equations [12,16] for the linearly elastic membrane after assuming that the only force exerted by the fluid to the vessel walls is the pressure of blood (ignoring shear stress) and that longitudinal displacements are negligible. The resulting (static) equation is

$$p(A) = G_0 \left( \left( \frac{A}{A_0} \right)^{1/2} - 1 \right)$$

where  $A_0$  is the unstressed (characteristic) cross-sectional area and  $G_0$  is the elasticity coefficient (proportional to the Young’s modulus). This gives linear relationship between the pressure and radius of a vessel. Using rigorous asymptotic analysis of the coupling between the Stoke’s flow and the Navier equations for the linearly elastic membrane it was shown in Reference [12] that the ‘independent ring model’ is the leading-order term in the approximation of the pressure in terms of the radial displacement.

To include the fact that the vessel radius changes slower at higher pressures (non-linear response, see e.g. Reference [5]) introduce parameter  $\beta$  and define

$$p(A) = G_0 \left( \left( \frac{A}{A_0} \right)^{\beta/2} - 1 \right) \quad (15)$$

where  $\beta > 1$  describes non-linear stress–strain response. Large  $\beta$  ( $\beta \rightarrow \infty$ ) corresponds to stiff walls. It was reported in References [10,11] that  $\beta = 2$  provides a ‘good fit’ with experimental data.

Each of the parameters in (15) can depend on  $x$  and  $t$ . In References [2,6] the Young’s modulus depends on  $x$  to account for the change in the elasticity properties of the channel wall in cases when an endovascular prosthesis is inserted in the vessel. In Reference [17] the coefficient  $G_0$  depends on both  $x$  and  $t$  to account for the fact that the stiffness of certain prostheses (self-expanding stents) depends on the strain and is a function of time [18]. In this paper we shall assume that  $G_0$  and  $\beta$  are constant. The unstressed cross-sectional area  $A_0$  will



be assumed constant except in Section 5 where we study the influence of vessel tapering on shock formation. There  $A_0$  will be a function of  $x$  and system (14) is then non-homogeneous.

We now have a closed system of partial differential equations given by (14) and (15). We will see in Section 4.1 that this system is strictly hyperbolic whenever the cross-sectional area is positive. We will prove that this can be guaranteed in the region of smooth flow whenever the initial and boundary cross-sectional area is greater than zero and the boundary velocity (pulsatile velocity profile on the inlet (proximal) boundary) satisfies certain *a priori* bounds. See Section 4.1. Although there are various types of initial–boundary value problems that are of interest in hemodynamics, in this paper we focus on the problem which is posed on the semi-infinite domain  $D = \{(x, t) \mid 0 < x < \infty, t \geq 0\}$  with the initial data prescribing the cross-sectional area and momentum (axial velocity) and the boundary data (on the left end of the domain) prescribing the pulsatile flow rate.

This problem is well posed and we will study the conditions on the initial and boundary data that guarantee blood flow without shock wave formation. In the next section, we first prove a theorem which provides sufficient conditions on the initial and boundary data that imply the existence of a smooth solution for a hyperbolic conservation law. The proof reveals the conditions which need to be satisfied for the existence of a smooth flow and provides the techniques necessary to estimate first shock formation for the data that do not satisfy the conditions from the theorem. We will see that the pulsatile flow rate boundary data typically lead to shock formation. However, for the data corresponding to a healthy individual, first shock formation occurs well outside the domain describing any section of the human circulatory system (2.8 m from the inlet boundary). See Section 4.

### 3. SMOOTH FLOW: THE GENERAL RESULT

In this section, we prove a theorem which provides conditions under which an initial–boundary value problem for a system of two quasilinear conservation laws admits a continuous solution. The approach is similar to that of Reference [23]. The proof is based on the study of the behaviour of the solution and its derivative along the characteristics [20,21]. The main assumption is that the system can be written in terms of the *characteristic variables*, or *Riemann invariants*.

We study a  $2 \times 2$  system of conservation laws

$$U_t + F(U)_x = 0, \quad x \in \mathbb{R}, \quad t > 0 \quad (16)$$

where  $U(t, x) \in \mathbb{R}^2$  and  $F: \mathbb{R}^2 \rightarrow \mathbb{R}^2$  is a smooth function of  $U$ . We shall assume that the system is strictly hyperbolic, that is, there exist two distinct eigenvalues,  $\lambda < \mu$ . We consider the above system in characteristic variables

$$z_t + \lambda(z, w)z_x = 0 \quad (17)$$

$$w_t + \mu(z, w)w_x = 0 \quad (18)$$

where  $z$  and  $w$ , the *characteristic variables* or *Riemann invariants*, are the unknown functions and  $\lambda$  and  $\mu$  are smooth functions of  $z$  and  $w$ . (We note that this reduction can always be

done locally.) Furthermore, we shall assume that system (16) is genuinely non-linear, that is  $\partial\lambda/\partial z \neq 0$  and  $\partial\mu/\partial w \neq 0$  in the domain under consideration.

Consider the following initial boundary-value problem on the domain  $D = \{(x, t) \mid t \geq 0, x_1(t) \leq x < \infty\}$

$$\begin{aligned} \text{at } t=0: \quad & z = z_0(x), \quad w = w_0(x) \quad (0 \leq x < \infty) \\ \text{on } x = x_1(t): \quad & w = g(t, z) \end{aligned} \quad (19)$$

where we have assumed, without the loss of generality, that  $x_1(0) = 0$ . We will show that under certain assumptions this initial-boundary value problem admits a (unique) continuous solution. The basic hypotheses are the following:

H1 (Smoothness of the data). Data  $w_0, z_0$  and  $g$  are  $C^1$  and the boundary  $x_1 \in C^2$ .

H2 (*A priori* estimates). The boundary  $x_1$  is non-characteristic. More precisely,  $\lambda(z, w) < x'_1(t) < \mu(z, w)$  on  $x = x_1(t)$  and

$$\mu(z, w) - x'_1(t) \geq M(T_0, Z, W), \quad \forall 0 \leq t \leq T_0, \quad \forall |z| \leq Z, \quad \forall |w| \leq W$$

where  $M(T_0, Z, W) > 0$ .

H3 (Initial data).  $\|(z_0, w_0)\|_{C_0}$  is bounded and  $z'_0(x) \leq 0, w'_0(x) \geq 0$  for  $0 \leq x < \infty$ .

H4 (Boundary data). The dependence of  $g$  on  $z$  is such that  $\partial g/\partial z \geq 0$ .

H5 (Eigenvalues). The eigenvalues satisfy  $\partial\lambda/\partial z < 0, \partial\mu/\partial w > 0$ .

H6 (Compatibility). The following compatibility conditions hold:

$$\begin{aligned} w_0(0) &= g(0, z_0(0)) \\ x'_1(0) - \mu(z_0(0), w_0(0))w'_0(0) &= \frac{\partial g}{\partial t}(0, z_0(0)) \\ &\quad + \frac{\partial g}{\partial z}(0, z_0(0))(x'_1(0) - \lambda(z_0(0), w_0(0))z'_0(0)) \end{aligned}$$

We state the theorem in a form which will be useful in providing information about the regimes in which the flow of blood modelled by (14) does not exhibit shock waves.

### Theorem 3.1

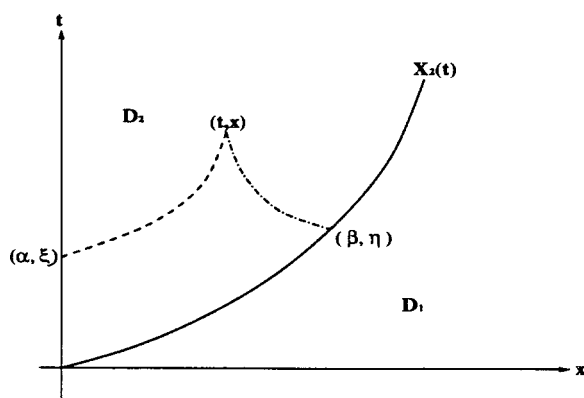
Suppose that hypotheses H1–H6 hold. If  $\partial q/\partial t \leq 0$  the initial boundary value problem (17), (19) admits a (unique) global  $C^1$  solution  $(z(t, x), w(t, x))$  on the domain  $D$ .

### Proof

Let  $x_2(t)$  be the forward characteristic emanating from the point  $x=0, t=0$ . Then hypotheses H3 and H5 imply that there exists a (unique) global  $C^1$  solution in the domain  $D_1 = \{(t, x) \mid x \geq x_2(t), t \geq 0\}$ . See Reference [19]. Furthermore, the behaviour of  $z$  along the characteristic  $x_2(t)$  passing through the origin is such that

$$\frac{dz}{dt}(t, x_2(t)) \leq 0 \quad (20)$$

In the rest of the proof we focus on the solution in the domain  $D_2 = \{(t, x) \mid t \geq 0, x_1(t) \leq x \leq x_2(t)\}$ . See Figure 1. We will show that for any fixed  $T_0 > 0$  and  $0 < T \leq T_0$ , the  $C^1$  norm of


 Figure 1. The subdomains  $D_1$  and  $D_2$  of the domain  $D$ .

the solution over the domain  $D^T = \{(t, x) \mid 0 \leq t \leq T, x_1(t) \leq x \leq x_2(t)\}$  is bounded independently of  $T$ , namely,  $\|(z, w)\|_{C^1(D^T)} \leq C(T_0)$ , where  $C(T_0) > 0$  is independent of  $0 < T \leq T_0$ . If there exists a global  $C^1$  solution, it has to satisfy this  $C^1$  estimate.

Let  $(t, x) \in D^T$ . To study the behaviour of the solution at the point  $(t, x)$  we will track the history of the solution and its derivative along the forward and backward characteristics passing through  $(t, x)$ . By hypothesis H2 any forward characteristic (with slope  $\mu > 0$ ) passing through  $(t, x)$  must intersect the boundary  $x_1$  at one and only one point; denote that point by  $(\alpha(t, x), \xi(t, x))$ . Similarly, since  $\lambda < \mu$ , any backward characteristic (with slope  $\lambda < 0$ ) must intersect the characteristic curve  $x_2$  at one and only one point; denote that point by  $(\beta(t, x), \eta(t, x))$ . Denote by  $z_0(t)$  the value of  $z$  along the characteristic boundary  $x_2$ . Then

$$z(t, x) = z_0(\beta(t, x)) \quad (21)$$

$$w(t, x) = g(\alpha(t, x), z(\alpha(t, x), \xi(t, x))) \quad (22)$$

Since  $\beta(t, x) \leq t$  we have

$$\|z\|_{C^0(D^T)} \leq C(T_0), \quad \forall (t, x) \in D^T \quad \text{with } 0 < T < T_0 \quad (23)$$

Now since  $\alpha(t, x) \leq t$ , Equation (22) and estimate (23) imply

$$\|w\|_{C^0(D^T)} \leq C(T_0), \quad \forall (t, x) \in D^T \quad \text{with } 0 < T < T_0 \quad (24)$$

This provides a uniform  $C^0$  estimates of the solution.

We proceed by getting uniform estimates of the solution derivatives by deriving the ordinary differential equations that are satisfied by the derivatives of the solution along the characteristic curves [19–21].

We first estimate  $\partial z / \partial x$ . Let

$$v = e^{k(z, w)} \frac{\partial z}{\partial x} \quad (25)$$

where  $k$  is defined by

$$\frac{\partial k}{\partial w} = -\frac{1}{\mu - \lambda} \frac{\partial \lambda}{\partial w} \quad (26)$$

Then one can derive the following ODE which is satisfied by  $v$  along the backward characteristic  $x'(t) = \lambda$  where  $z$  is constant

$$\frac{dv}{dt} \equiv \frac{\partial v}{\partial t} + \lambda(z, w) \frac{\partial v}{\partial x} = -e^{k(z, w)} \frac{\partial \lambda}{\partial z} v^2 \quad (27)$$

The corresponding initial condition, given on  $x_2(t) = \mu(w_0, z_0(t))$ , reads  $v|_{x_2} = eI^k(\partial z/\partial x)|_{x_2}$ . We can simplify this by noting that on  $x_2$  the following holds  $z'_0(t) = \partial z/\partial t + \mu(\partial z/\partial x)$ . Since  $\partial z/\partial t = -\lambda \partial z/\partial x$  we get that  $\partial z/\partial x = [1/(\mu - \lambda)]z'_0(t)$  on  $x_2$ . Therefore, the initial condition can now be written as

$$v|_{x_2} = \frac{e^{k(w_0, z_0(t))}}{(\mu - \lambda)(w_0, z_0(t))} z'_0(t) \quad (28)$$

The initial-value problem (27) and (28) has a solution  $v$  which is given by

$$v(t, x) = \frac{e^{k(w_0, z_0(\beta))} z'_0(\beta)}{B(t, \beta(t, x))}$$

where

$$B(t, \beta) = (\mu - \lambda)(w_0, z_0(\beta)) + z'_0(\beta) e^{k(w_0, z_0(\beta))} \int_{\beta}^t \frac{\partial \lambda}{\partial z}(w(\tau, \tilde{x}(\tau, \beta)), z_0(\beta)) e^{-k(w(\tau, \tilde{x}(\tau, \beta)), z_0(\beta))} d\tau$$

Here  $x = \tilde{x}(\tau, \beta)$  denotes the backward characteristic passing through the point  $(\beta, \eta)$ . By hypothesis H2 we have that  $\mu - \lambda$  is bounded uniformly away from zero, and since  $z'_0 \partial \lambda/\partial z \geq 0$  (hypotheses H3 and H5) we conclude that  $B$  is never zero and we obtain a uniform bound of  $v$  and then of  $\partial z/\partial x$ :

$$\left| \frac{\partial z}{\partial x}(t, x) \right| \leq C(T_0), \quad \forall (t, x) \in D^T, \quad 0 < T \leq T_0$$

Furthermore, we get that  $\text{sign } \partial z/\partial x = \text{sign } z'_0(t) = -1$ .

Next we estimate  $\partial w/\partial x$  by performing the following three steps:

*Step 1* (The sign of  $\partial w/\partial x$  on  $x = x_1(t)$ ): Differentiate the boundary condition  $w = g(t, z)$  along  $x = x_1(t)$  and calculate

$$\frac{\partial w}{\partial x} = \frac{1}{x'_1(t) - \mu} \left[ \frac{\partial g}{\partial t} + \frac{\partial g}{\partial z} (x'_1(t) - \lambda) \frac{\partial z}{\partial x} \right] \quad \text{along } x = x_1(t) \quad (29)$$

Now, since  $\lambda < x'_1(t) < \mu$ ,  $\text{sign}(\partial z/\partial x) = \text{sign}(z'_0(t))$  and  $\partial g/\partial z > 0$ , and by taking into account the assumption  $\partial g/\partial t \leq 0$ , we get that  $\partial w/\partial x \geq 0$  on  $x_1(t)$ .

*Step 2* (The sign of  $\partial w/\partial x$  in  $D^T$ ): Since  $w$  is constant along the forward characteristic we have  $w(t, x) = w(\alpha(t, x), \xi(t, x))$ ,  $\forall (t, x) \in D^T$ , where  $\xi(t, x) = x_1(\alpha(t, x))$ . Therefore,

$$\frac{\partial w}{\partial x}(t, x) = \frac{\partial w}{\partial t}(\alpha, \xi) \frac{\partial \alpha}{\partial x}(t, x) + \frac{\partial w}{\partial x}(\alpha, \xi) \frac{\partial \xi}{\partial x}(t, x) = (x'_1(t) - \mu) \frac{\partial w}{\partial x}(\alpha, \xi) \frac{\partial \alpha}{\partial x}(t, x)$$

To determine the sign of  $\partial w/\partial x$  in  $D^T$  we first notice that  $x'_1 - \mu < 0$  and  $\partial w/\partial x(\alpha, \xi) \geq 0$ . Furthermore, from the definition of  $\alpha = \alpha(t, x)$  we see that  $\alpha$  decreases as  $x$  increases, and so  $\partial \alpha/\partial x \leq 0$ . Therefore, in  $D^T$  we have  $\text{sign } \partial w/\partial x \geq 0$ .

*Step 3* (The  $C^0$  estimate of  $\partial w/\partial x$  in  $D^T$ ): Let  $u = e^{h(z, w)} \partial w/\partial x$  where  $\partial h/\partial z = [1/(\mu - \lambda)] \partial \mu/\partial z$ . Function  $u$  satisfies the following ODE along the characteristic  $x' = \mu$

$$\frac{du}{dt} = -e^{-h(z, w)} \frac{\partial \mu}{\partial w} u^2$$

and initial condition  $u(\alpha, \xi) = e^{h(z(\alpha, \xi), w(\alpha, \xi))} \partial w/\partial x(\alpha, \xi)$  given on  $x_1(t)$  at  $(\alpha(t, x), \xi(t, x))$ . By integration we get

$$u(t, x) = \frac{e^{h(z(\alpha, \xi), w(\alpha, \xi))} \partial w/\partial x(\alpha, \xi)}{A(t, \alpha)} \quad (30)$$

where

$$A(t, \alpha) = 1 + \frac{\partial w}{\partial x}(\alpha, \xi) e^{h(z(\alpha, \xi), w(\alpha, \xi))} \int_{\alpha}^t \frac{\partial \mu}{\partial w}(z(\tau, \tilde{x}(\tau, \alpha)), w(\alpha, \xi)) e^{-h(z(\tau, \tilde{x}(\tau, \alpha)), w(\alpha, \xi))} d\tau \quad (31)$$

where  $x = \tilde{x}(\tau, \alpha)$  is the forward characteristic passing through the point  $(\alpha, \xi)$ . Since  $\partial \mu/\partial w \geq 0$  (hypothesis H5) and  $\partial w/\partial x \geq 0$  on  $x_1(t)$  (Step 1) we see that  $A(t, \alpha)$  is never zero. The uniform estimate for  $\partial w/\partial x$  on  $D^T$  follows from hypothesis H2, and from the uniform estimates of  $z, w$  and  $\partial z/\partial x$  in  $D^T$ . This completes the proof.  $\square$

In the next section we shall use the estimates presented in the above proof to determine the time and the location of the first shock formation in the model of blood flow (14) with pulsatile boundary condition on the left boundary. The main reason for why the solution breaks down is positive inflow rate at the beginning of each systole which does not satisfy the main assumption of the theorem that the left boundary condition  $g$  is decreasing in time  $\partial g/\partial t \leq 0$ . Our estimates will show, however, that in a healthy individual shock waves never form in any subsection of the blood circulatory system since the location of the first shock formation is well outside the physiologically interesting domain (2.8 m downstream from the heart).

#### 4. IMPLICATIONS FOR BLOOD FLOW

In this section, we present a detailed analysis of Equations (14) describing blood flow in complaint vessels. Since the equations are quasilinear, it is not clear *a priori* that the system is always hyperbolic. In Section 4.1 we derive the conditions on the initial and boundary data that guarantee strict hyperbolicity. The conditions are quite reasonable: the cross-sectional area of the vessel initially and on the left boundary should never be equal to zero and the pulsatile velocity profile (prescribed on the left (proximal) boundary) must satisfy certain *a priori*

bounds. We will see that those *a priori* bounds will be satisfied in a healthy individual since the blood flow velocity is typically much smaller than the speed at which signals propagate through the abdominal aorta. Next we investigate the flow regimes in which shock waves never form. We present those results in Section 4.2. Finally, in Section 4.3 we show that pulsatile data will typically give rise to shock formation in a semi-infinite compliant vessel but the location of the first shock formation is well outside the physiologically interesting domain. We derive an estimate which predicts shock formation location and time, and in Section 5 show that they are in excellent agreement with the numerical simulations.

Since it was shown in Section 2 that the source term is of one order of magnitude smaller than the effects of non-linear advection, the estimates of the first shock formation are obtained with the zero source term. This corresponds to the inviscid flow, namely,  $\nu=0$ . Since the inviscid flow does not generate boundary layer it is physically reasonable to assume the so-called flat velocity profile (plug flow). This corresponds to taking the coefficient  $\alpha$  in Equations (14) equal to 1. We point out that these simplifying assumptions are going to be used only in this section of the paper. It will be shown in Section 5 that the shock formation estimate presented in this section is in a good agreement with the numerical simulation obtained with a non-zero source term and physiologically reasonable values of  $\nu$  and  $\alpha$  ( $\nu=3.2 \times 10^{-6} \text{ m}^2/\text{s}$  and  $\alpha=1.1$ ).

Write system (14) with zero source term in quasilinear form

$$\begin{pmatrix} A_t \\ m_t \end{pmatrix} + \begin{pmatrix} 0 & 1 \\ -\frac{m^2}{A^2} + \frac{1}{\rho} A p'(A) & \frac{2m}{A} \end{pmatrix} \begin{pmatrix} A_x \\ m_x \end{pmatrix} = \begin{pmatrix} 0 \\ 0 \end{pmatrix} \quad (32)$$

The eigenvalues are

$$\lambda = U - \sqrt{\frac{1}{\rho} A p'(A)} = U - \sqrt{\frac{G_0 A}{\rho A_0}}, \quad \mu = U + \sqrt{\frac{1}{\rho} A p'(A)} = U + \sqrt{\frac{G_0 A}{\rho A_0}} \quad (33)$$

where  $U = m/A$  is the axial velocity. The right and left eigenvectors are given by

$$r_\lambda = \begin{pmatrix} 1 \\ \lambda \end{pmatrix}, \quad r_\mu = \begin{pmatrix} 1 \\ \mu \end{pmatrix}, \quad l_\lambda = \begin{pmatrix} -\mu \\ 1 \end{pmatrix}, \quad l_\mu = \begin{pmatrix} -\lambda \\ 1 \end{pmatrix} \quad (34)$$

To use the results from Section 3 we diagonalize the system by calculating the Riemann invariants. Let  $z$  be the Riemann invariant for which  $\nabla z \cdot r_\mu = 0$  and  $w$  such that  $\nabla w \cdot r_\lambda = 0$ . By integration one obtains

$$z = 2\sqrt{\frac{G_0}{\rho} \frac{A}{A_0}} - U, \quad w = 2\sqrt{\frac{G_0}{\rho} \frac{A}{A_0}} + U \quad (35)$$

The diagonalized system reads

$$\begin{aligned} z_t + \lambda(z, w) z_x &= 0 \\ w_t + \mu(z, w) w_x &= 0 \end{aligned} \quad (36)$$

We study solutions of the initial boundary-value problem on the domain  $D = \{(t, x) \mid t \geq 0, 0 \leq x < \infty\}$  with the initial and boundary data given by

$$\begin{aligned} \text{Initial data} \quad z &= z_0(x), \quad w = w_0(x) \\ \text{Boundary data} \quad w &= g(t, z) = z + 2U_{\text{pul}}(t) \end{aligned} \quad (37)$$

where  $U_{\text{pul}}(t)$  is the pulsatile flow rate,  $U_{\text{pul}} \in C^1$ , and  $z_0, w_0 \in C^1$ . In our numerical simulations, see Section 5, we use the pulsatile flow rate obtained using trigonometric functions (FFT) to fit the physiological pulsatile flow rate data presented in Reference [22]. Furthermore we shall assume that

$$z'_0(x) \leq 0, \quad w'_0(x) \geq 0, \quad z_0(x) \geq z_{0\min} > 0, \quad w_0(x) \leq w_{0\max} \quad (38)$$

*Remark 4.1*

In terms of the conserved quantities  $A$  and  $m = AU$  conditions (38) read

$$\begin{aligned} z'_0(x) &= \frac{d}{dx} \left( \sqrt{\frac{G_0 A(0, x)}{\rho A_0}} - U(0, x) \right) \leq 0, \quad w'_0(x) = \frac{d}{dx} \left( \sqrt{\frac{G_0 A(0, x)}{\rho A_0}} + U(0, x) \right) \geq 0 \\ z_0(x) &= \frac{G_0 A(0, x)}{\rho A_0} - U(0, x) \leq 0, \quad w_0(x) = \frac{G_0 A(0, x)}{\rho A_0} + U(0, x) \leq w_{0\max} \end{aligned}$$

If the initial data is constant,  $A(0, x) = A_0$  and  $U(0, x) = 0$  for example, the sign of  $z_{0\min}$  is consistent with  $G_0 A(0, x) / \rho A_0 > 0$ .

To analyse the solutions of this initial boundary-value problem we first show that under certain reasonable assumptions on the initial and boundary data system (14) is strictly hyperbolic.

#### 4.1. Strict hyperbolicity

We investigate the conditions under which the eigenvalues  $\lambda$  and  $\mu$  of the Jacobian of system (14) satisfy  $\lambda(z, w) < \mu(z, w)$ . We found that this system has an interesting property, similar to a model describing compressible isentropic gas dynamics: if the system is strictly hyperbolic initially and on the left boundary, then it stays strictly hyperbolic everywhere in the domain of the existence of a smooth solution. Furthermore, we derive the conditions on the initial and boundary data which imply strict hyperbolicity on the left boundary and show that these conditions are quite reasonable if, for example, constant initial data are considered.

First note that Equations (33) imply that system (14) ceases to be strictly hyperbolic if  $A = 0$  (this corresponds to the vacuum state in gas dynamics). Let  $D^T = \{(t, x) \mid 0 \leq t \leq T, 0 \leq x < \infty\}$  denote the existence domain of a continuous and piecewise  $C^1$ -solution.

#### Theorem 4.2

Suppose that the left boundary  $x_1(t) = 0$  is non-characteristic (i.e.  $\lambda < x'_1 < \mu$ ). If  $A(0, x) > 0$  initially, and if  $A(t, x_1(t)) > 0$  on the left boundary, then  $A(t, x) > 0, \forall (t, x) \in D^T$ , and so system (14) is strictly hyperbolic in  $D^T$ .

*Proof*

Let  $x=x(t)$  be a solution curve of the ODE  $dx/dt=U(t,x)$ . The first equation in (14) implies that along  $x=x(t)$  the cross-sectional area satisfies  $dA/dt=-A(\partial U/\partial x)$ , where  $dA/dt=\partial A/\partial t+U\partial A/\partial x$  denotes the derivative along  $x=x(t)$ . Suppose that  $(t^*,x^*)\in D^T$  is such that  $A(t^*,x^*)=0$ . This implies  $\lambda=\mu=U(t^*,x^*)$  at  $(t^*,x^*)$ . From the definition of the eigenvalues (33) we see that up to  $(t^*,x^*)$  the integral curve  $x=x(t)$  passing through  $(t^*,x^*)$  lies between the characteristic curves through  $(t^*,x^*)$ . Therefore, it either intersects the  $t=0$  axis or it intersects the left boundary. Suppose that  $x=x(t)$  intersects the initial line  $t=0$ ; denote that point by  $(0,x(t^*,x^*))=(0,x_0)$ . The solution of the ODE satisfied by  $A$  along  $x=x(t)$  is given by  $A(t^*,x^*)=A(0,x_0)e^{-\int_0^{t^*}(\partial U/\partial x)d\tau}$ , and we see that  $A(t^*,x^*)=0$  if and only if  $A(0,x_0)=0$  which contradicts the assumption that initially  $A(0,x)>0$  for all  $x$ . The same reasoning applies to the case when  $x=x(t)$  intersects the left boundary. This concludes the proof.  $\square$

*Proposition 4.3*

The following conditions on  $U(t)|_{x_1=0}$  and on  $z_0(x)$  guarantee that the assumptions of Theorem 4.2 are satisfied:

$$1. \quad -\frac{1}{3}z_{0\min} < U(t) < z_{0\min} \quad \text{implies} \quad \lambda < x'_1 < \mu \quad \text{on} \quad x_1=0 \quad (39)$$

$$2. \quad U(t) > -z_{0\min} \quad \text{implies} \quad A(t,0) > 0 \quad (40)$$

*Proof*

To show that (39) implies  $\lambda < x'_1 < \mu$  we first note that  $\sqrt{G_0 A/(A_0 \rho)} = (w+z)/4$ . Therefore,

$$\lambda|_{x_1(t)=0} = U(t) - \frac{1}{4}(w+z)|_{x_1(t)=0} = U(t) - \frac{1}{4}(2z + 2U(t)) < U(t) - \min z_0(x)$$

Since  $U(t) < z_{0\min}$  we obtain  $\lambda|_{x_1(t)=0} < 0$ . Similarly,

$$\mu|_{x_1(t)=0} = U(t) + \frac{1}{4}(w+z)|_{x_1(t)=0} = U(t) + \frac{1}{4}(2z + 2U(t)) > \frac{1}{2}(3U(t) + \min z_0(x))$$

which is positive due to the first inequality in (39).

To see that (40) implies  $A(t,0) > 0$  we first note that  $A(t,0)=0$  if and only if  $w+z=0$  at  $x_1(t)=0$ . Since  $w+z=2z(t,0)+2U(t)$  on  $x_1=0$ , condition (40) implies that  $w+z>0$  on the left boundary.  $\square$

*Corollary 4.4*

System (14) is strictly hyperbolic if the initial data  $(z_0, w_0)$  and the boundary data  $U(t)$  are such that

$$w_0(x) + z_0(x) > 0 \quad (\text{this is equivalent to } A(0,x) > 0) \quad (41)$$

$$-\frac{1}{3}z_{0\min} < U(t) < z_{0\min} \quad (42)$$

*Remark 4.5*

In terms of the conserved quantities  $A$  and  $m$ , assuming, for simplicity, constant initial data,  $A(0,x)=A_0$  and  $m(0,x)=0$ , where  $A_0$  is the unstressed cross-sectional area, condition (42)



requires that the velocity  $U(t)$  prescribed on the left boundary is such that  $-1/3\sqrt{G_0/\rho} < U(t) < \sqrt{G_0/\rho}$ . Considering that the expected average velocity is an order of magnitude smaller than  $\sqrt{G_0/\rho}$ , this is rather reasonable. (The sound speed in this model is much larger than the magnitude of the (averaged) blood velocity.) For the pulsatile flow boundary data considered in Section 5, and for the values of  $G_0$  corresponding to a healthy individual, see Section 5 and Reference [22], this condition is always satisfied.

#### 4.2. Existence of a global smooth solution

In this section we use Theorem 3.1 to derive the conditions under which there exists a smooth solution of the initial boundary-value problem studied in this paper. In other words, we rephrase the existence theorem, Theorem 3.1, in terms of the quantities and data arising in the blood flow problem modeled by (14), or equivalently, by Equations (36).

##### Theorem 4.6

Consider the initial boundary-value problem (36), (37) where the initial and boundary data satisfy conditions (38), (41) and the compatibility conditions

$$\begin{aligned} w_0(0) &= z_0(0) + 2U(0) \\ -\mu(z_0(0), w_0(0))w'_0(0) &= 2U'(0) - \lambda(z_0(0), w_0(0))z'_0(0) \end{aligned} \quad (43)$$

Furthermore, let

$$U(t) \geq -\frac{1}{4}z_{0\min} \quad (44)$$

Then if

$$U'(t) \leq 0 \quad \forall t \geq 0 \quad (45)$$

the problem admits a (unique) piecewise  $C^1$ -solution.

##### Proof

First notice that conditions (41) imply that the system is strictly hyperbolic. We next show that all the hypotheses of Theorem 3.1 are satisfied. Hypotheses H1, H3, H4 and H6 are a direct consequence of the definition of the blood flow problem under consideration. Hypothesis H2 is satisfied because (41) and (44) hold. More precisely, on  $x_1(t)=0$  we have

$$\mu(z, w) - x'_1(t) = \frac{3}{4}w - \frac{1}{4}z = \frac{3}{4}(z + 2U(t)) - \frac{1}{4}z \geq \frac{1}{2}z_{0\min} + \frac{3}{2}U(t) \geq \frac{1}{8}z_{0\min} > 0$$

Hypothesis H5 holds after we express the eigenvalues in terms of the Riemann invariants

$$\lambda = \frac{1}{4}w - \frac{3}{4}z, \quad \mu = \frac{3}{4}w - \frac{1}{4}z \quad (46)$$

to see that  $\partial\lambda/\partial z = -\frac{3}{4} < 0$ , and  $\partial\mu/\partial w = \frac{3}{4} > 0$ . Finally, since  $\partial g/\partial t = U'(t) \leq 0$ , Theorem 3.1 implies the existence of a global piecewise  $C^1$ -solution.  $\square$

##### Remark 4.7

We draw a parallel between the behaviour described in Theorem 4.6 and a problem in compressible gas dynamics. Imagine a piston, originally located at the origin, moving with speed  $U(t)$  in a tube which is assumed to be infinite, and that the gas on the right side of the

piston is isentropic. Assuming that the piston movement does not create a vacuum state, and assuming that there was no vacuum state initially, if the acceleration of the piston is negative, the flow driven by the piston will be smooth for all time.

#### 4.3. Shock wave formation

In the case when the left boundary data corresponds to the pulsatile flow rate, assumption (45) of Theorem 4.6 is not satisfied. Shock waves form because the flow rate has a large positive gradient. As we shall see in this subsection, the time of the first shock formation depends on the Young's modulus, and on the magnitude of the derivative of the pulsatile flow rate. In this section, we estimate the time and location of the first shock formation and comment on the physiological meaning of our findings.

Since the entire flow is driven by the pulsatile flow we can consider simple initial data which are such that the conditions from the previous section (to guarantee, for example, strict hyperbolicity) are satisfied. We consider constant (unstressed) initial data

$$A(0, x) = A_0, \quad U(0, x) = 0 \quad (47)$$

which in terms of the Riemann invariants read  $w_0(x) = z_0(x) = 2\sqrt{G_0/\rho}$ . For this set of initial data  $z$  is constant everywhere in the region of smooth flow; the characteristics are straight lines in  $D_2 = \{(t, x) \mid t \geq 0, x_2(t) \leq x < \infty\}$ , where  $x_2(t)$  is the forward characteristic  $x'_2 = \mu$  emanating from  $(0, 0)$ . The solution in region  $D_1 = \{(t, x) \mid t \geq 0, 0 \leq x \leq x_2(t)\}$ , bounded by the left boundary  $x_1 = 0$  and the forward characteristic  $x_2$ , is driven by  $U(t)$  on  $x_1$  and will develop shock waves due to the fact that  $U'(t)$  changes sign. In fact, the pulse corresponding to the systole starts with a high positive gradient  $U'(t) > 0$ , which will give rise to the shock formation at some time  $t_s$ , at the location  $x_s$  where  $x_s/t_s = \mu(z_0, w_0)$ .

To estimate the time  $t_s$  we note that at the point  $(t_s, x_s)$  the partial derivative  $\partial w / \partial x$  blows up. This occurs at the point where the denominator  $A(t, \alpha)$  in (30) becomes equal to zero. The denominator  $A(t, \alpha)$  can be calculated from equation (31) by recalling that  $\partial \mu / \partial w = 3/4$  and that  $z = z_0$  everywhere. This implies that in (31)  $e^{h(z(\alpha, \xi), w(\alpha, \xi)) - h(z(\tau, \xi(\tau, \alpha)), w(\alpha, \xi))} = 1$  and so  $A(t, \alpha) = 1 + \frac{3}{4} \partial w / \partial x(\alpha, \xi)(t - \alpha)$ . From Equation (29) we see that  $\partial w / \partial x|_{x_1=0} = -2U'(t)/\mu + (\lambda/\mu) \partial z / \partial x$ . Since  $\partial z / \partial x = 0$ , we obtain

$$A(t, \alpha) = 1 - \frac{3}{2} \frac{U'(t)}{\mu} (t - \alpha) \quad (48)$$

Therefore, the first time the shock forms is equal to

$$t_s = \alpha + \frac{U(t) + \sqrt{G_0 A / \rho A_0}}{(3/2) U'_{\text{pul}}(t)} \quad (49)$$

#### Proposition 4.8

Assuming constant initial data, the time  $t_s$  of the first shock formation is given by (49).

Equation (49) indicates that the steeper the pulse, the sooner and closer the shocks will form. Keener and Sneyd obtained a similar result in Reference [23] (although less general). They comment that this behaviour may be related to the pistol-shot which can be heard through a stethoscope in patients with aortic insufficiency, but not in other patients. Another implication of our results is that the shocks will form sooner if the walls of the vessel are

less rigid. This will allow faster decrease in the cross-sectional area  $A$  as a result of the low diastolic pressure.

We conclude this section by obtaining an estimate for the location  $x_s$  of the first shock formation in the model of blood flow through the abdominal aorta between renal and iliac arteries. The elasticity modulus  $G_0$  measured for this portion of the aorta is obtained from Reference [22] and is estimated to be  $G_0 = 4 \times 10^4 \text{ N/m}^2$ . Blood density is taken to be  $\rho = 1050 \text{ kg/m}^3$ . We are using pulsatile flow boundary data with the measurements obtained from Reference [22], approximated by the trigonometric functions using fast Fourier transform. All the figures in Section 5 include the calculated approximation of the pulsatile flow rate in one cardiac cycle. We obtain that  $\max U'(t)$  occurs at the beginning of each systole, and is estimated to be equal to  $86 \times 10^{-1} \text{ m/s}^2$ . This data gives rise to the cross-sectional area  $A(t, x)$  which is of the same order of magnitude as the unstressed cross-sectional area  $A_0$ . Therefore, using (49) we obtain

$$t_s \approx \frac{\sqrt{40000/1050}}{1.5 \times 8.6} = 0.478 \text{ s} \quad \text{and} \quad x_s = t_s \mu = 0.478 * \sqrt{40000/1050} = 2.95 \text{ m} \quad (50)$$

which is well outside any physiologically relevant subdomain of the circulatory system. In particular, it is outside the domain corresponding to the abdominal aorta between renal and iliac arteries whose length is of the order of 10 cm.

## 5. NUMERICAL INVESTIGATION

In this section, we investigate shock formation in the solution of system (14) using numerical simulations. We show that our theoretical predictions are in excellent agreement with the results obtained using numerical simulations. In addition to the issues analysed in the previous sections of the paper in this section we also study the influence of vessel tapering on shock formation. We obtain a surprising result which shows that tapering of the vessel postpones shock formation. We provide an argument for why this is the case.

The numerical solutions were obtained using the Richtmyer two step Lax Wendroff method, as described in Reference [24]. We use Strang splitting to deal with the source term.

We describe the numerical method in Section 5.1, we present the results related to the shock formation in compliant vessels with constant unstressed radius in Section 5.2 and analyse shock formation in tapered compliant vessels in Section 5.3.

### 5.1. The numerical method

We write Equations (14) in conservation form and solve using the two-step Lax–Wendroff method. We take into account that  $A_0$  can depend on  $x$  and write the equations in conservation form as follows:

$$\frac{\partial}{\partial t} U + \frac{\partial}{\partial x} F = S \quad (51)$$

where

$$U = \begin{bmatrix} A \\ m \end{bmatrix}, \quad F(U) = \begin{bmatrix} 0 \\ \frac{\alpha m^2}{A} + \frac{G_0 \beta}{\rho(\beta + 2)} \left( \frac{A}{A_0} \right)^{\beta/2+1} A_0 \end{bmatrix} \quad (52)$$

and

$$S(U) = \begin{bmatrix} 0 \\ -2 \frac{\alpha}{\alpha - 1} \frac{m}{A} + \frac{G_0 \beta}{\rho(\beta + 2)} \left( \frac{A}{A_0} \right)^{\beta/2+1} A_0' \end{bmatrix} \quad (53)$$

The eigenvalues of the Jacobian of  $F$  are

$$\lambda_{1,2} = \frac{\alpha m}{A} \pm \sqrt{\alpha(\alpha - 1) \left( \frac{m}{A} \right)^2 + \frac{G_0 \beta}{2\rho} \left( \frac{A}{A_0} \right)^{\beta/2}} \quad (54)$$

When  $A_0 = A_0(x)$  is variable, the flux function and the source term also depend on  $x$  and the system of conservation laws is no longer homogeneous. We solve an initial boundary-value problem defined on the computational domain  $D = (0, L)$  with the initial conditions  $A = A(x, 0) = A_0$  and  $m = m(x, 0) = 0$ , and the boundary data corresponding to the pulsatile velocity profile on the left boundary, and the ‘transparent boundary condition’ on the right end.

We apply the two-step Lax–Wendroff method. Assume that the grid is uniform with  $\Delta x$  denoting the mesh width and  $\Delta t$  the time step. Define  $U_m^n$  to be the approximation of the solution at  $(m\Delta x, n\Delta t)$ . The method takes the form

$$U_m^{n+1} = U_m^n - \frac{\Delta t}{\Delta x} (F(U_{m+1/2}^{n+1/2}) - F(U_{m-1/2}^{n+1/2})) + \frac{\Delta t}{2} (S(U_{m+1/2}^{n+1/2}) + S(U_{m-1/2}^{n+1/2}))$$

where

$$U_j^{n+1/2} = \frac{U_{j+1/2}^n + U_{j-1/2}^n}{2} + \frac{\Delta t}{2} \left( -\frac{F(U_{j+1/2}^n) - F(U_{j-1/2}^n)}{\Delta x} + \frac{S(U_{j+1/2}^n) + S(U_{j-1/2}^n)}{2} \right)$$

for  $j = m + \frac{1}{2}$  and  $j = m - \frac{1}{2}$ .

The method is stable if the CFL condition

$$\max |\lambda_{1,2}| \frac{\Delta t}{\Delta x} = \max \left| \frac{\alpha m}{A} \pm \sqrt{\alpha(\alpha - 1) \left( \frac{m}{A} \right)^2 + \frac{G_0 \beta}{2\rho} \left( \frac{A}{A_0} \right)^{\beta/2}} \right| \frac{\Delta t}{\Delta x} < 1$$

is satisfied.

The data used in the simulation are: blood density  $\rho = 1050 \text{ kg/m}^3$ , viscosity  $\nu = 3.2 \times 10^{-6} \text{ m}^2/\text{s}$  and unstressed radius of the abdominal aorta  $R_0 = 0.0082 \text{ m}$ . The elasticity coefficient  $G_0 = 4 \times 10^4 \text{ N/m}^2$  is obtained from Reference [22] with  $\beta = 2$ . The time step used in all the simulations is  $\Delta t = 3.18 \times 10^{-4}$ .

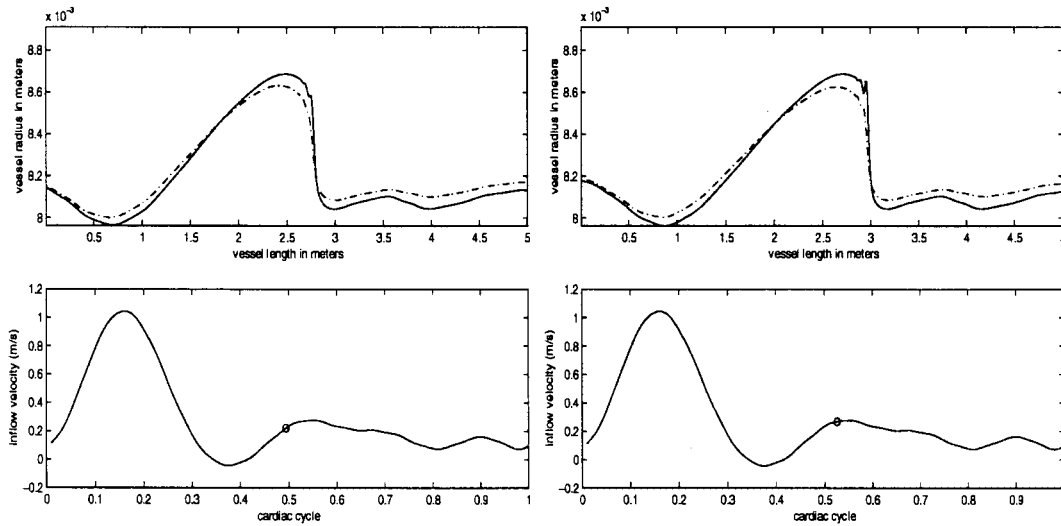


Figure 2. Shock formation in the system with the zero source term (solid line) and with the source term given by  $f_v$  in (13) (dashed line). The two pictures on the left show that the first shock formation in the system with the zero source term occurs at 2.8 m downstream from the inlet boundary. As the little circle at the bottom picture indicates, this corresponds to roughly 0.49 s in the cardiac cycle. The figures on the right show shock formation in the system with the non-zero source term (dashed line) which occurs roughly at 3 m downstream from the inlet boundary, at about 0.51 s in the cardiac cycle.

### 5.2. Shock formation in a straight compliant vessel

We are assuming here that the unstressed cross-sectional area  $A_0$  is constant. We are going to present two studies. One concerns shock formation in system (14) with the zero source term, and the other includes the source term  $f_v$  given by (13) which accounts for the viscous effects. Our numerical simulations will show that:

1. in the system with the zero source term the first shock develops around 2.8 m downstream from the inlet boundary (which is around 0.49 s in the cardiac cycle); this is in a very good agreement with the predictions in Section 4;
2. in the system with the source term given by  $f_v$  in (13), the time and the location of the first shock formation is slightly delayed ( $t = 0.51$  s in the cardiac cycle) and the shock is located around 3 m downstream from the inlet boundary; this is in accordance with the non-dimensional analysis presented in Section 2 which shows that the source term is of one order of magnitude smaller than the rest of the system. Thus, the analysis of the first shock formation based on the zero source term provides a good estimate for the first shock formation in (14).

Figure 2 shows the radii profiles along a 5-m long vessel, at two instances: 0.49 and 0.51 s in the cardiac cycle. The solid curve describes the radius profile obtained in the simulation of system (14) with the zero source term. The dashed curve describes the solution of the system with the source term given by  $f_v$  in (13). Notice that the radius depicted with the solid curve develops a shock sooner, indicating that the small (negative) source  $f_v$  slightly

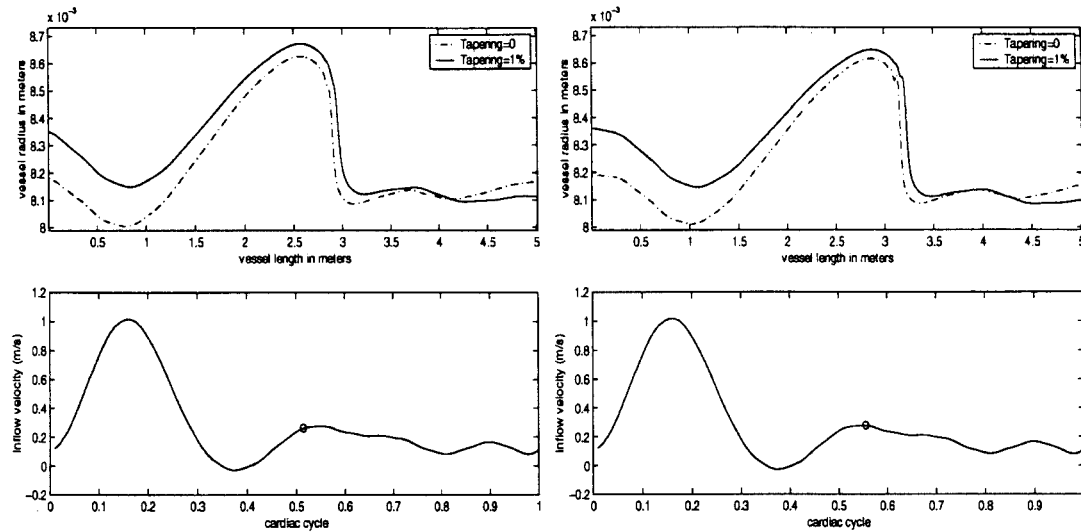


Figure 3. Shock formation in the system with zero tapering (dashed line) and with the tapering of 1% (solid line). The two pictures on the left show the corresponding radii (top) and the moment in the cardiac cycle (bottom) when the first shock (dashed line) is formed. As the little circle indicates, this corresponds to roughly 0.51 s in the cardiac cycle. The two pictures on the right show the same information taken at 0.57 s in the cardiac cycle when the second shock (solid line) develops.

postpones shock formation. The radius profile steepens as the pulse travels through the vessel. Roughly at 2.8 m the radius profile develops a shock.

### 5.3. Shock formation in a tapered compliant vessel

We are assuming here that  $A_0(x)$  is a decreasing function of  $x$ . In the numerical simulations presented here we have assumed that  $A_0(x)$  is a linear function of  $x$  of the form

$$A_0(x) = A_0 - T * A_0 * x$$

where  $0 \leq T < 1$  is the 'tapering factor' and  $A_0 = (0.0082 \text{ m})^2$  is the unstressed cross-sectional area used in the previous section. All the numerical simulations from this point on will be performed with the non-zero source term.

An approach based on the non-dimensional analysis presented in Section 2, or simply a comparison between the magnitudes of the source terms  $f_v$  and the source term arising due to the variable cross-section (see (5.3)) given by

$$f_{A_0} = \frac{G_0 \beta}{\rho(\beta + 2)} \left( \frac{A}{A_0} \right)^{\beta/2+1} A'_0$$

implies that tapering of less than 1% per metre ( $T = \mathcal{O}(10^{-3})$ ) gives the source term which is of the same magnitude or smaller than  $f_v$ . Therefore, there will be little change in the location of the shock formation due to the tapering of less than 1%. In Figure 3 we compare the solutions obtained using numerical simulation of Equations (14) with the variable unstressed

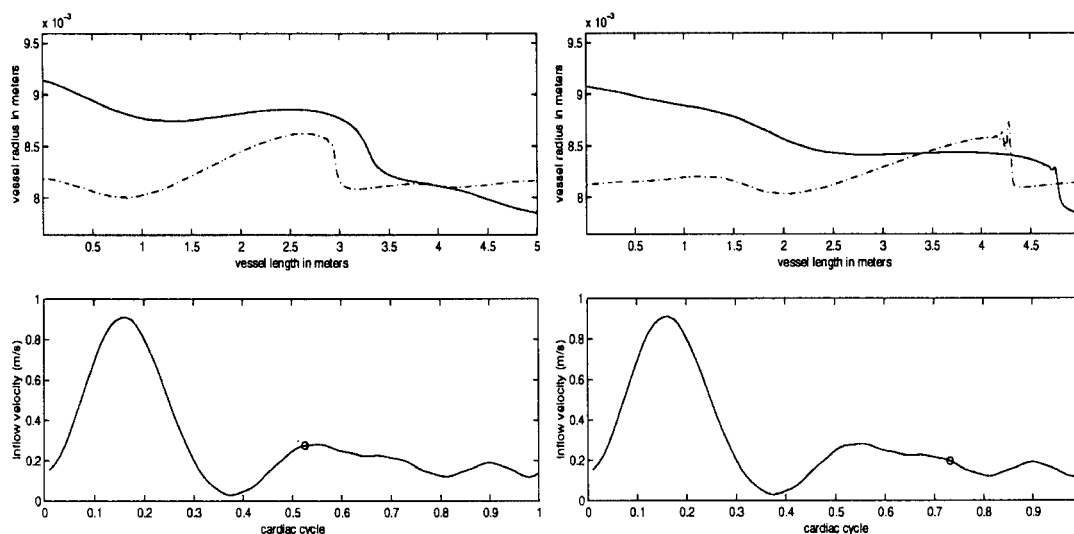


Figure 4. Shock formation in the system with zero tapering and with the tapering of 5%. The two pictures on the left show the corresponding radii (top) and the moment in one cardiac cycle (bottom) when the first shock (zero tapering) is about to form. As the little circle indicates, this corresponds to roughly 0.51 s in the cardiac cycle. The two pictures on the right show the same information taken at 0.72 s in the cardiac cycle when second shock (5% tapering) is beginning to develop at 4.7 m downstream from the inlet boundary.

cross-sectional area  $A_0(x)$  where the tapering factor is precisely 1% per metre,  $T = 0.01$  (solid line) and the solution with zero tapering (dashed line). In all the simulations here the source term which accounts for the viscosity,  $f_v$ , has been taken into account. The shock in the tapered vessel starts to develop around 0.57 s in a cardiac cycle at 3.3 m downstream from the inlet boundary. We draw the following two conclusions: first, the first shock formation in a tapered vessel with the tapering factor of less than 1% per metre is close to the first shock formation in a non-tapered vessel, as expected; second, shock formation in tapered vessels is delayed. This is surprising because the behaviour uncovered here is opposite to the expected behaviour of the piston driven compressible flow in rigid tubes. Recall that in Section 3 we compared the structure of the equations studied here to the equations of compressible gas dynamics describing the piston driven flow in a rigid tube. It is well known that decreasing cross-sectional area of the rigid tube in the piston driven flow will give rise to compression in the solution and shocks will form sooner. To confirm the delaying effect of the vessel tapering in the blood flow model, we ran numerical simulations with 5% tapering. Indeed, Figure 4 shows that in a tapered vessel (solid line) with  $T = 0.05$  the first shock develops at around 4.7 m downstream from the inlet boundary, which is around 0.72 s in the cardiac cycle. Movies showing shock formation can be found on [www.math.uh.edu/~canic/hemo/shocks](http://www.math.uh.edu/~canic/hemo/shocks).

Postponed shock formation can be explained by a combination of two phenomena: (1) transmural pressure rises as the cross-sectional area decreases (see (15)) and (2) signals travel faster in tapered vessels (see (4)). High transmural pressure in tapered vessels in turn gives rise to the larger cross-sectional area and this new increase in cross-sectional area

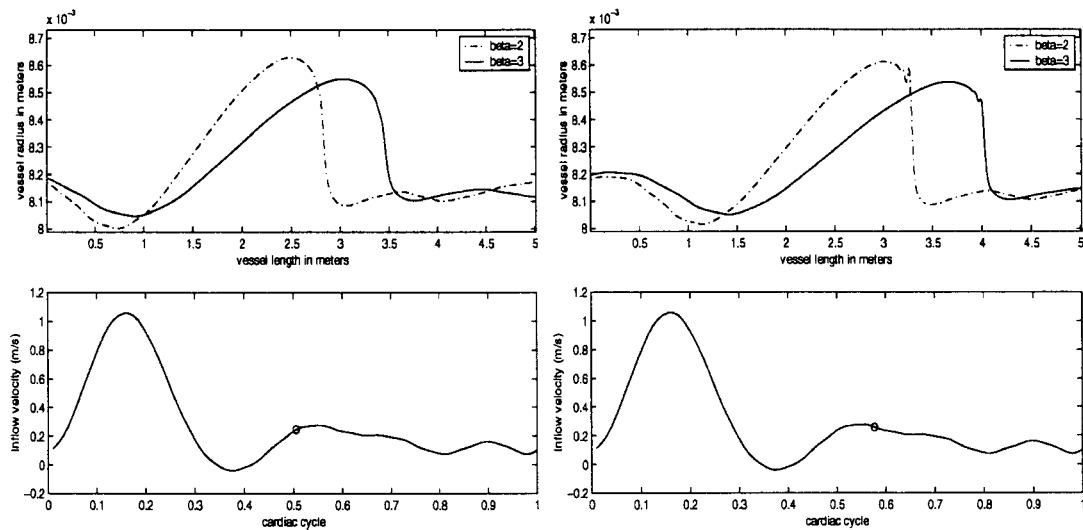


Figure 5. Shock formation comparison between the models with  $\beta=2$  and 3. The two pictures on the left show the corresponding radii (top) and the moment in one cardiac cycle (bottom) when the first shock ( $\beta=2$ ) has just formed. As the little circle indicates, this corresponds to roughly 0.5s in a cardiac cycle. The two pictures on the right show the same information taken at 0.59s in a cardiac cycle when the second shock ( $\beta=3$ ) has just formed.

travels fast through the entire vessel, but still in a ‘tapered’ fashion. See Figure 4. This allows higher volume flow through the channel and thus later shock formation. This is a crucial place where the two problems (the piston driven compressible flow through the channel with fixed walls and the ‘pulsatile flow driven’ incompressible flow through compliant vessels) differ substantially.

Notice that if we use Equation (49) to estimate the time of the first shock formation even in the case when the unstressed cross-sectional area is variable, smaller  $A_0$  leads to the later shock formation, which is consistent with our findings. Keep in mind, however, that Equation (49) was obtained by assuming that  $A_0$  is constant. For small deviations in  $A_0$  Equation (49) should still provide a good estimate for  $t_s$ .

We conclude this section by a comment related to the influence of parameter  $\beta$ , describing the linear/non-linear response of the vessel wall, on shock formation. As mentioned in Section 2, the limit  $\beta \rightarrow \infty$  corresponds to stiff walls, and large  $\beta$  will lead to early ‘saturation’ in radial displacement. In other words, higher pressure difference  $\Delta p$  is needed for a given radial displacement difference  $\Delta R$ ,  $R > R_0$ , in case of a larger  $\beta$ . Furthermore, the expression for the eigenvalues (4) indicates that the magnitude of the eigenvalues increases with increasing  $\beta$ , which means that signals travel faster through stiffer walls (although with smaller amplitudes). Finally, if we use Equations (50) and (49) to estimate the location of the first shock formation, we see that in stiff vessels shocks form further downstream from the inlet boundary. This is supported by the numerical simulations presented in Figure 5. Notice that even for a small difference in the parameter  $\beta$ , namely  $\beta=2$  vs 3, the difference in the location of the first shock formation is rather pronounced (2.9 m vs 4 m downstream from the inlet boundary).



This is because signals travel faster in stiffer vessels and because first shock forms later in stiffer vessels. Figure 5 also indicates radial wall deformations are smaller in stiffer vessels.

## 6. CONCLUSION

In this paper, we discussed some basic mathematical issues related to the initial boundary-value problem for a quasilinear system of hyperbolic equations (14) modelling pulsatile blood flow in large vessels. We focused on the quasilinear effects such as shock formation in straight and tapered compliant vessels, and *a priori* estimates which guarantee strict hyperbolicity of the equations. The results presented here are useful not only in the mathematical understanding of the model equations, but also in the numerical simulation. Knowing the estimates on the initial and boundary data which guarantee strict hyperbolicity is important, for example, for the stability of finite difference methods. On the other hand, understanding the influence of the data on shock formation is crucial for the simulation of the underlying equations using a finite element method.

Our motivation for this study came from a related problem: understanding the flow of blood and optimal design of self-expanding prostheses (stents) in endovascular treatment of abdominal aneurysm. In order to study aspects of blood flow after the insertion of an endovascular prosthesis, it is necessary to first understand the properties of blood flow prior to the procedure. This is where the results presented in the present paper became indispensable.

We point out that the model considered in this work incorporates many simplifications from the real application. They include the ‘closure’ assumption on the shape of the velocity profile, the ‘independent ring model’ pressure–radius relationship for the description of the wall behaviour and the axi-symmetric geometry of the domain. However, because of its importance, simplicity and wide appearance in the literature we felt that a rigorous analysis and understanding the quasilinear effects of the underlying model was crucial in further studies of blood flow through large, axi-symmetric vessels.

## ACKNOWLEDGEMENTS

The authors would like to thank Andro Mikelić, Luca Formaggia, Dragan Mirković and Alfio Quarteroni for their input and encouragement. The authors would also like to thank Howard Levine for his expedite handling of the manuscript. Most of all, many thanks to the referees for their patience and valuable comments.

## REFERENCES

1. Anliker M, Rockwell R. Nonlinear analysis of flow pulses and shock waves in arteries. *Zeitschrift für Angewandte Mathematik und Mechanik* 1971; **22**:217–246.
2. Formaggia L, Nobile F, Quarteroni A. A one-dimensional model for blood flow: application to vascular prosthesis. In *Mathematical Modelling and Numerical Simulation in Continuum Mechanics, Lecture Notes in Computational Science and Engineering 19*, Babuska I, Ciarbet PG, Miyoshi T (eds). Springer-Verlag: Berlin, 2001.
3. Formaggia L, Nobile F, Quarteroni A, Veneziani A. Multiscale modeling of the circulatory system: a preliminary analysis. *Computing and Visualization in Science* 1999; **2**:75–83.
4. Olufsen M, Peskin C, Kim W, Pedersen E, Nadim A, Larsen J. Numerical simulation and experimental validation of blood flow in arteries with structured-tree outflow conditions. *Annals of Biomedical Engineering* 2000; **28**:1281–1299.

5. Peskin C. *Partial Differential Equations in Biology*. Courant Institute of Mathematical Sciences, Lecture Notes, New York, 1975.
6. Čanić S. Blood flow through compliant vessels after endovascular repair: wall deformations induced by the discontinuous wall properties. *Computing and Visualization in Science* 2002; **4**(3):147–155.
7. Čanić S, Mirković D. A hyperbolic system of conservation laws in modeling endovascular treatment of abdominal aortic aneurysm. *Hyperbolic Problems: Theory, Numerics, Applications* 2000; **141**(1):227–236.
8. Barnard ACL, Hunt WA, Timlake WP, Varley E. A theory of fluid flow in compliant tubes. *Biophysical Journal* 1966; **6**:717–724.
9. White F. *Viscous Fluid Flow*. McGraw-Hill: New York, 1986.
10. Smith NP, Pullan AJ, Hunter PJ. The generation of an anatomically accurate geometric coronary model. *Annals of Biomedical Engineering* 2000; **28**(1):14–25.
11. Smith NP, Pullan AJ, Hunter PJ. An anatomically based model of transient coronary blood flow in the heart. *SIAM Journal of Applied Mathematics* 2002; **62**(3):990–1018.
12. Čanić S, Mikelić A. Effective equations describing the flow of a viscous incompressible fluid through a long elastic tube. *Comptes Rendus de l'Académie des Sciences, Serie I* 2002; 661–666.
13. Hilbert D. An efficient Navier–Stokes solver and its applications to fluid flow in elastic tubes. *Colloquia Societatis Janos Bolyai* 1987; **50**:423–431.
14. Perktold K, Rappitsch G. Mathematical modeling of local arterial flow and vessel mechanics. In *Computational Methods for Fluid Structure Interaction*, Crolet J, Ohayon R (eds), Pitman Research Notes in Mathematics No. 306. Longman: Harlow, 1994; 230–245.
15. Quarteroni A, Tuveri M, Veneziani A. Computational vascular fluid dynamics: problems, models and methods. *Computing and Visualization in Science* 2000; **2**:163–197.
16. Čanić S, Mikelić A. Effective equations modeling the flow of a viscous incompressible fluid through a long elastic tube arising in the study of blood flow through small arteries. *SIAM J. Appl. Dyn. Sys.*, submitted.
17. Čanić S. The influence of self-expanding stents on the blood flow after endovascular repair, in preparation.
18. Wang R, Ravi-Chandar K. Mechanical response of a metallic aortic stent. (*EMRL Report Number*: 01-01), Center for Mechanics of Solids, Structures and Materials The University of Texas at Austin.
19. Ta-tsien L. Global classical solutions for quasilinear hyperbolic systems. In *Research in Applied Mathematics*, Ciarlet PG, Lions L-L (series eds). Wiley: New York, 1994.
20. Lax PD. Hyperbolic systems of conservation laws ii. *Communications on Pure and Applied Mathematics* 1957; **10**:537–556.
21. Lax PD. Development of singularities of solution of nonlinear hyperbolic partial differential equations. *Journal of Mathematical Physics* 1964; **5**:611–613.
22. MacSweeney STR, Young G, Greenhalgh RM, Powel JT. Mechanical properties of the aneurysmal aorta. *British Journal of Surgery* 1992; **79**:1281–1284.
23. Keener J, Sneyd J. Mathematical physiology. *Interdisciplinary Applied Mathematics*, vol. 8. Springer: New York, 1998.
24. LeVeque RJ. *Numerical Methods for Conservation Laws*. Birkhäuser: Boston, 1992.
25. Fung YC. *Biomechanics: Mechanical Properties of Living Tissues*. Springer: New York, 1993.